IEEE Copyright Notice

Date of publication: May 26, 2021

DOI: 10.1109/TPS.2021.3080681.

Cite as:
Yamasaki H., Nomura S., Xun X., Kuroki T., Kang J., Yagi T., and Okubo M., Toward NO_x/SO_x and Nanoparticle Control Technology Using a Single-Stage Wet-Type Nonthermal Plasma Reactor. IEEE Tran. Plasma Sci., Vol. 49, No. 6, pp. 1860–1870 (2021).

Toward NO_x/SO_x and Nanoparticle Control Technology Using a Single-Stage Wet-Type Nonthermal Plasma Reactor*

Haruhiko Yamasaki[1], Shunto Nomura[1], Xi Xun [1], Tomoyuki Kuroki[1], Jinkyu Kang[2], Tadao Yagi[3], and Masaaki Okubo[1]

[1]Department of Mechanical Engineering, Osaka Prefecture University, 1-1 Gakuen-cho, Naka-ku, Sakai 599-8531, Japan

[2]Samsung Advanced Institute of Technology, Samsung Electronics Co., Ltd., 130 Samsung-ro, Yeongtong-gu, Suwon-si, Gyeonggi-do, 16678, Korea

[3]MD2 laboratory, Samsung R&D Institute Japan, 2-7 Sugasawa-cho, Tsurumi-ku, Yokohama 230-0027, Japan

Abstract Nitrogen oxides (NO_x), sulfur oxides (SO_x), and particulate matter (PM) emitted by diesel engines, thermal power generation plants, and various industrial establishments have had unfavorable effects on the environment globally. Therefore, it is necessary to install aftertreatment systems on such combustors because the emissions cannot be treated for combustion improvement only. To establish NO_x/SO_x, and nanoparticle control technologies, herein, we propose a single-stage wet-type nonthermal plasma (NTP) reactor. To evaluate the performance of the proposed system, we conducted a laboratory-scale experiment with a mixture of NO_x, SO_x, and polystyrene particles. In this system, PM is collected in a water film by the electrostatic effect, NO is oxidized to NO_2 by NTP, and NO_2 and SO_2 are absorbed into a water film on the inner wall of the reactor. We achieved almost complete and simultaneous removal of the pollutants, with a partial collection efficiency of more than 98% for the nanoparticles (diameter = 22–334 nm), removal efficiency of 98% for NO_x, and removal efficiency of 99% for SO_x. Further, we proposed a method to treat the chemical components left in the water film to enable a self-sustaining technique. The technology allows for conserving in space and investment costs in exhaust gas aftertreatment facilities.

Keywords: Nitrogen oxides, nonthermal plasma, particulate matter, sulfur oxides, wet-type plasma reactor.

Haruhiko Yamasaki (email corresponding author)
Department of Mechanical Engineering, Graduate School of Engineering, Osaka Prefecture University, 1-1 Gakuen-cho, Naka-ku, Sakai 599-8531, Japan.
E-mail: hyamasaki@me.osakafu-u.ac.jp

*The final publication of this paper is
Yamasaki H., Nomura S., Xun X., Kuroki T., Kang J., Yagi T., and Okubo M., Toward NO_x/SO_x and Nanoparticle Control Technology Using a Single-Stage Wet-Type Nonthermal Plasma Reactor. IEEE Tran. Plasma Sci., Vol. 49, No. 6, pp. 1860–1870 (2021). https://doi.org/ 10.1109/TPS.2021.3080681.

Introduction

Air pollutants, including particulate matter, nitrogen oxides NO_x (=NO + NO_2), and sulfur oxides (SO_x), still remain significant social and environmental problems in East Asian countries. Nitrogen oxide is produced mainly when oxygen and nitrogen in the air are combined by burning fuels at high temperatures (thermal NO_x), and the main sources of NO_x are emissions by diesel engines, thermal power generation plants, and various industrial establishments. NO_x and SO_x are also the precursors of fine particulate matter (PM) or $PM_{2.5}$ [1], [2]. Specifically, smaller particles having aerodynamic dimensions of approximately 100 nm diameter induce respiratory diseases because they can be inhaled into the distal regions of the lungs and deposited there to induce disease. To reduced air pollutants, it is necessary to install aftertreatment systems on the source combustors because the emissions cannot be treated for combustion improvement only. Currently, selective catalytic reduction (SCR) [3], [4] followed by wet flue gas desulfurization (FGD) using chemical agents, such as calcium carbonate ($CaCO_3$) and sodium hydroxide (NaOH) [5], [6], are the available technologies for NO_x and SO_2 reduction. These are applied globally for the flue gas treatments of coal-fired and oil-fired thermal power plants. However, high-performance and low-cost technologies are desired in developing countries. SCR cannot be applied in several industries, such as glass manufacturing, because of significant catalyst choking due to the impurities in the flue gases [7]. Furthermore, SCR can selectively convert NO_x into nitrogen and water, but its efficiency significantly decreases at lower temperatures, and its use is limited. For example, for NO_x SCR in the garbage incinerator aftertreatment [8], the flue gas temperature is further increased using a heater before the gas passes through the SCR catalyst. For these reasons, the development of smaller-sized, cost-effective, and lower-temperature simultaneous removal techniques for NO_x, SO_2, and PM are desired, and a wet-type nonthermal plasma (NTP) reactor is proposed in this study as an effective means. NO_x reduction can occur rapidly at room temperature and atmospheric pressure without catalysts with NTP, such as corona discharge [9–13] and dielectric barrier discharge [14–16], and the wet combined process of NO oxidation and absorption using ozone [17]. Moreover, the simultaneous removal of NO_x and SO_2 can be realized by a combined technique of NTP and wet reduction [18–21]. A method combining NTP, wet reduction, and electrostatic precipitator (ESP) has been proposed [22–25] for the removal of PM, NO_x, and SO_x, but few studies have addressed simultaneous removal of these pollutants using the same single-stage system. Our previous research has shown that the wet-type NTP reactor with an aqueous solution film of a mixture of NaOH and Na_2SO_3 can remove NO_x, SO_x, and particles simultaneously with negligible reaction byproducts, such as N_2O, CO, HNO_2, and HNO_3 [22]. In the reported work, the details of PM removal efficiency are not investigated, but the performance of NO_x and SO_x removal by different aqueous solutions is described. Another study has shown PM removal performance by the wet-type NTP reactor with varying water-film and electrical-discharge parameters [23]. However, the details of NO_x and SO_x removal efficiencies are not investigated. In our previous research, we evaluated the removal performance of NO_x and SO_x of a wet-type NTP reactor without chemical additives [24]. By reacting and dissolving NO_2 and SO_2 with a water film, NO_x and SO_x were removed, but nitrate (NO_3^-) and nitrite (NO_2^-) ions still remained in the water. It is found that NO_3^- and NO_2^- could be removed by applying argon plasma to the water

containing the ions using a wet-type plasma reactor [25]. Therefore, if the wet-type plasma reactor can remove PM, NO_x, and SO_x using only water without chemical additives, exhaust gas facilities can reduce space and investment costs owing to the simple structure. SO_x components retained in the water after treatment in the wet-type plasma reactor can be treated with desulfurizing agents, such as calcium carbonate ($CaCO_3$) and sodium hydroxide (NaOH). However, in these previous works, removal of NO_x and SO_x and removal of nanoparticles were achieved separately. The influence of nanoparticle collection by ESP on NO_x and SO_x removal is not clarified. Furthermore, detailed parameter effects, such as water flow rate and applied voltage, and their characteristics concerning the simultaneous removal of nanoparticles, NO_x, and SO_x were not investigated.

In the present study, we performed simultaneous removal experiments on PM, NO_x, and SO_x using a wet-type NTP reactor with varying water-film and electrical-discharge parameters. Furthermore, we evaluated simultaneously the size-dependent or partial collection efficiency for nanoparticles and removal efficiencies of NO_x and SO_x. To understand the characteristics of the wet-type plasma reactor, the physical properties of water were measured during processing.

Principle of simultaneous removal

Wet-type plasma reactor

Fig. 1 shows the schematic of the wet-type plasma reactor used in the experiment. The right side of the figure shows an overview of the reactor, and the left side shows the detailed view of the plasma region. In the right side of the figure, the reactor consists of a quartz tube, a stainless-steel wire (discharge electrode), liquid silver paste (grounded electrode), an overflow tank, a bottom tank, a storage tank, a liquid pump, and a flow controller. The quartz tube is a vertically placed circular pipe with an inner diameter of 20 mm, outer diameter of 25 mm, and a length of 646 mm; it is covered with silver paste to a width of 260 mm and thickness of 0.05 mm. The stainless-steel wire of 2.0 mm diameter is placed along the central position of the quartz tube. Then, distilled water is allowed from an overflow tank in the upper region of the quartz tube and flows over the quartz tube's inner wall to generate the water film. NTP is generated by applying a pulsed high voltage to the discharge electrode. The water film uniformly flows on the quartz tube's inner wall because this surface is hydrophilic owing to the NTP. Under constant applied voltage, the presence of a water film allows current to flow more easily to the ground electrode and increases the discharge power compared to the case without a water film. In the proposed technique, NO_x is absorbed into the water film as nitric acid and nitrous acid by air plasma, SO_2 is also absorbed by the water film, and PM is collected in the water film by electrostatic precipitation.

As shown in the detailed view of the plasma region in the left side of the figure, the PM that enters the electric field formed by the discharge electrode develops a positive charge and migrates away from the discharge electrode toward the ground electrode. When positively charged particles reach the tube's inner wall with the ground electrode, the positive charge is neutralized, and the particles are carried downstream by the water film. Thus, gaseous air pollutants flowing in the channel are treated. The water passing through the quartz tube is stored in the bottom tank and sent to the overflow tank using a

pump via the storage tank so that the water circulates through this closed channel during the experiments. In the case of simultaneous removal of NO_x, SO_x, and PM, it is especially necessary to consider interactions, such as changes in the electrical conductivity of the nitrate due to absorption of SO_x and oxidation of NO by nitric acid or sulfuric acid.

Chemical reactions

The NO gaseous component passing through the wet-type plasma reactor reacts with nitrogen and oxygen radicals as well as ozone. Although some of the NO is reduced to N_2 by the reactions (1) and (2), most of the NO is oxidized to NO_2 by the ozone and oxygen radical ·O, as shown in reactions (3) and (4).

$$N_2 + e^- \rightarrow \cdot N + \cdot N + e^- \quad (1)$$

$$NO + \cdot N \rightarrow N_2 + \cdot O \quad (2)$$

$$NO + O_3 \rightarrow NO_2 + O_2 \quad (3)$$

$$NO + \cdot O + M \rightarrow NO_2 + M \quad (4)$$

where ·N and ·O are radicals, e- is an electron, M is a third-body substance, and N_2 and O_2 are molecules in air. When water is present in the air, the OH radicals generated by plasma decomposition react with the NO and NO_2 to form nitric acid (HNO_3) and nitrous acid (HNO_2), respectively, as shown in reaction (5) and (6).

$$NO + OH + M \rightarrow HNO_2 + M \quad (5)$$

$$NO_2 + OH + M \rightarrow HNO_3 + M \quad (6)$$

Here, NO_2 and SO_2 are water soluble and therefore dissolve in water to produce H_2SO_3, HNO_2, and HNO_3, as shown in reaction (7) and (8).

$$SO_2 + H_2O \rightarrow H_2SO_3 \quad (7)$$

$$2NO_2 + H_2O \rightarrow HNO_2 + HNO_3 \quad (8)$$

A previous study [25] reported that nitrate and nitrite ions in solution are reduced by Ar plasma treatment. Thus, it is possible to reduce the nitrate and nitrite ions in solution by switching from air plasma to argon plasma after the treatment of PM, NO_x, and SO_x in gas. The reduction of the nitrate and nitrite ions was also proposed using a mixed alkaline solution of NaOH and urea ($CO(NH_2)_2$) [26]. With this method, it may be possible to not only reduce the nitrate and nitrite ions by $CO(NH_2)_2$ but also remove sulfate ions by NaOH. Therefore, we considered that an environmentally friendly system could be constructed using NaOH and $CO(NH_2)_2$ solutions for the aftertreatment of liquid wastes from the experimental apparatus.

Experimental apparatus and method

An overview of the experimental setup is depicted in **Fig. 2**. Synthesized air (O_2 = 21% and N_2 = 79%) and an N_2-based gas mixture of NO and SO_2 (NO = SO_2 = 200 ppm) are mixed to prepare simulated exhaust gases in Flow 1 (air + NO+ SO_2) type flow. In the Flow 2 type flow, a test aerosol is generated by passing air through an aerosol generator (Model 3076, TSI Inc.) containing a solution of a mixture of polystyrene latex with six types of average polystyrene particle diameters, namely 29, 47, 61, 100, 202, and 303 nm

(SC-0030-A, SC-0051-D, SC-0060-D, and SC-024-S for 29, 47, 61, and 202 nm, respectively, JSR Co.; 3100A and 3300A for 100 and 303 nm, respectively, Thermo Fisher Scientific Co. Ltd.). The particle distribution simulates the particulate matter in diesel exhaust gas. After Flow 2 containing the polystyrene particles passes through a gas dryer, it is mixed with Flow 1 containing air, NO_x, and SO_x at a mixing point. The mixed gas flows into the reactor from the upper inlet of the plasma reactor.

The experiment is performed with a total flow rate of 4 L/min (2 L/min each in Flow 1 and Flow 2) adjusted through mass-flow controllers (SFC280E, Hitachi Metal Co.). An insulated gate bipolar transistor power supply (PPCP Pulsar SMC-30/1000, 500 W, Masuda Research Inc.) is used as the reactor power supply, and nonequilibrium NTP is generated by applying high-voltage pulses between the stainless-steel wire of the discharge electrode and silver paste of the grounded electrode. The pulse frequency f is set to 210 Hz for all experiments. The instantaneous waveforms of the applied peak voltage V, current I, and power $V \times I$ are measured using a voltage probe (P6015A, conversion factor = 1 V/kV, Sony Tektronix Inc.), a current probe (P6021, conversion factor = 10 A/V, Sony Tektronix Inc.), and a digital oscilloscope (DLM2054, 500 MHz and 2.5 GS/s, Yokogawa Electric Co.), respectively. The concentrations of the NO_x, SO_x, and O_2 are measured with a gaseous analyzer (PG-350, Chemiluminescence detection for NO_x, Infrared absorption for SO_x, Zirconia type measurement for O_2, Horiba Ltd.), and N_2O is measured using appropriate analyzers (VIA-510, Infrared absorption, Horiba Ltd.). The ozone is measured using a gas-detection tube (18M, Gastec Co.) placed between the heater and reactor. Because the ozone is generated by plasma when a voltage is applied, the ozone is removed by the heater (KRO-14K, Isuzu Seisakusho Co., Ltd) set to 250 °C downstream of the reactor. The PM is analyzed using a scanning mobility particle sizer (SMPS) (differential mobility analyzer (DMA): Model 3080 + condensation particle counter (CPC): Model 3787, measurement range of particle size: 10 to 414 nm, TSI Inc.). The concentrations of NO_3^- and NO_2^- in water are measured with a visible spectrophotometer (Colorimeter CO7500, Biochrom Ltd.) with color reagents (Nitrite and Nitrate, Kyoritsu Chemical-Check Lab., Co.). The pH and conductivity of water are measured using a compact water quality meter (MM-43X, Toadkk, Co. Ltd.), pH electrode (GST-5841C, Toadkk Co. Ltd.), and conductivity electrode (CT-58101B, Toadkk Co. Ltd.). The temperature of ground electrode wall is measured using an infrared thermometer (73036, Shinwa Rules Co. Ltd.).

Experimental results and discussion

Voltage and current waveforms

Fig. 3 shows the typical waveforms of the voltage v, current i, and instantaneous power $v \times i$ for the plasma reactor. The discharge mode is pulsed dielectric barrier discharge (DBD). In the time region where the voltage increases rapidly, a local streamer with a very strong electric field originates from the discharge electrode and reaches the ground electrode, causing the current to increase with oscillation. After that, the current decreases with the voltage decreases. The time-averaged discharge power P is calculated as an integral of the instantaneous power $v \times i$ of the positive area over a single period by multiplying the conversion factors of the voltage and current probes as well as pulse frequency f. When the applied peak voltage is set to 28 kV, as shown in the figure, the

time-averaged discharge power of the air plasma is equal to 31 W. For the wet-type NTP reactor, the flowing current is relatively large, exceeding 20 A, whereas for the dry-type NTP reactor, it is usually less than 15 A. **Fig. 4** shows the relationship between the discharge power and applied voltage at different flow rates of the water film q = 50, 100, and 200 mL/min. The pulse frequency is set to f = 210 Hz, and the gas flow rate is set to Q = 4 L/min. In this experiment, the applied voltage ranges from 26 to 32 V, and the discharge power ranges from 12 to 32 W. At q = 100 mL/min, the discharge power for V = 27 kV is almost the same as that for V = 26 kV because the amount of ions absorbed by the water film is lower when the applied voltage is lower. In such case, the discharge becomes unstable and the variation of the power becomes larger.

Partial collection efficiency

Fig. 5 shows the typical particle size distribution of nanoparticles introduced into the reactor when the flow rate of the water film is q = 100 mL/min. The vertical axis represents the normalized concentration ($dN/d\log D_p$), where D_p is the electrical mobility or Stokes diameter of particle. From **Fig. 5**, it is confirmed that the particle size distribution corresponds to the diameters of the six different polystyrene particles.

Fig. 6 shows the measured results for the size-dependent or partial collection efficiency of particles in the diameter range of 22–334 nm. The pulse frequency is again set to f = 210 Hz, and the gas flow rate is set to Q = 4 L/min. The voltage V and flow rate of the water film q are varied, and the SMPS measurements are started 4 min after the plasma is turned on, for a duration of 2 min; these procedures are repeated three times. Thus, a total of 6 min of measurements are obtained, with further gaseous component measurements later, as shown in **Figs. 8–10**. The error bars in the figures correspond to $\pm\sigma$, where σ is the standard deviation of the three measurements. In the figure, the collection efficiency is observed to decrease for smaller (< 30 nm) and larger particle (>300 nm) diameter ranges. There are three possible reasons for this: 1) the number of particles is low, 2) the measurement accuracy slightly decreases in these ranges, and 3) the plasma reactor generates other aerosols. Discussion regarding reason 3) is presented later in this section using the explanation for **Fig. 7**. It is seen from **Fig. 6(a)** that the average collection efficiencies in the measured diameter range are high and equal to 97, 98, and 98% at voltages of 26, 27, and 28 kV, respectively, when the water-film flow rate is q = 200 mL/min. In particular, the collection efficiencies for particle sizes ranging from 25 to 150 nm are maintained at approximately 95% or higher when the voltage is equal to or greater than 26 kV. It is seen from **Fig. 6(b)** that the average collection efficiencies in the measured diameter ranges are high and almost equal at 98, 98, and 97% for voltages of 26, 27, and 31 kV, respectively, when the flow rate of the water film q is 100 mL/min. Specifically, the collection efficiencies for particle sizes ranging from 25 to 220 nm are maintained at approximately 95% or higher when the voltage is equal to or greater than 26 kV. It is seen from **Fig. 6(c)** that the average collection efficiencies in the measured diameter ranges are high and almost equal at 95, 98, and 98% for voltages of 29, 31, and 32 kV, respectively, when the water-film flow rate is 50 mL/min. Here, the collection efficiencies for particle sizes ranging from 30–200 nm are maintained at approximately 95% or higher when the voltage is equal to or greater than 29 kV. As seen in **Fig. 6(a)–(c)**, the collection efficiency tends to decrease for diameters less than 20 nm and greater than

200 nm, which is attributable to the decrease in the initial number of particles or measurement accuracy.

To evaluate the influence of NO_x and SO_x inclusion in the gas on PM collection efficiency, the PM collection efficiency in the present study, including NO_x and SO_x, is compared with that in a previous study [23] without NO_x and SO_x inclusion. The result for q = 100 mL/min is shown in **Fig. 7**, and the partial collection efficiencies for representative particle sizes of 30, 50, 102, 202, and 300 nm are compared. As shown in the figure, at particle sizes less than 200 nm, the differences in the collection efficiencies are small and more than 98%. However, at 202 and 300 nm, the collection efficiency is decreasing owing to the formation of nitric acid and sulfuric acid mists [27], which could be generated by the discharge in the downstream region of the plasma reactor.

NO_x and SO_x removal efficiencies

Fig. 8 shows the time-dependent gaseous concentrations of the components NO_x, NO, NO_2, N_2O, SO_2, and O_2 when plasma is generated for a higher water-film flow rate of 200 mL/min. The measurements for the particle collection in **Fig. 6(a)** and gaseous components in **Fig. 8** are performed simultaneously. When distilled water with a low electrical conductivity (–30 μS/cm) is used as the water film, the discharge between the electrodes becomes unstable. Therefore, SO_2 is dissolved in the water film at a flow rate of 200 mL/min at time t = –10 min before the plasma is turned on so that the electrical conductivity of the water film is increased. After the dissolution of SO_2 for 10 min, the plasma is turned on at t = 0 min, and the treatment is performed for 10 min. As shown in **Fig. 8(a)**, owing to the effects of NO oxidization by plasma, followed by the absorption of NO_2 and SO_2 by the water film, NO decreases from 96 ppm to 0 ppm, NO_x decreases from 97 ppm to 8 ppm, and SO_2 decreases from 98 ppm to 1 ppm at an applied voltage of 28 kV and discharge power of 31 W. Consequently, NO_x removal efficiency of 92% or higher and SO_x removal efficiency of 98% are achieved. As shown in **Fig. 8(b)**, NO decreases from 98 ppm to 1 ppm, NO_x decreases from 101 ppm to 17 ppm, and SO_2 decreases from 92 ppm to 1 ppm at an applied voltage of 27 kV and discharge power of 26 W. Hence, the system achieves NO_x removal efficiency of 83% or higher and SO_x removal efficiency of 98% or higher. Furthermore, as shown in **Fig. 8(c)**, NO decreases from 96 ppm to 1 ppm, NO_x decreases from 100 ppm to 1 ppm, and SO_2 decreases from 90 ppm to 0 ppm at an applied voltage of 26 kV and discharge power of 12 W. Consequently, the system achieves NO_x removal efficiency of 96% or higher and SO_x removal efficiency of 99%. Despite the lower applied voltage of V = 26 kV, NO_x removal efficiency is higher than that on other voltage conditions. This is because pH value at t = 0 was higher than that on the other voltage conditions at the applied voltage of 26 kV, as shown in **Fig. 12(a)**, which is presented later in this session. Because the water film can absorb NO_2 more efficiently with higher pH, NO_x removal efficiency is higher. In **Fig. 8(a)** and **(b)**, the concentrations of NO_2 and NO_x slightly increase with time after the plasma treatment. This phenomenon could be attributed to the desorption of NO_2 absorbed in the water film. It is known that as the pH of the solution decreases with increase in the elapsed time, NO_2 is induced by conversion of nitrite ions, resulting in the generation of NO and NO_2 at the gas–liquid interface. Therefore, it is essential to maintain a higher pH in the solution. **Fig. 8(a)–(c)** show that N_2O is generated by the reaction

between NO_2 and N radicals or by the reaction between N_2 and O radicals. However, N_2O concentrations are less than 10 ppm in all cases and much lower than that of the removed NO_x.

Fig. 9 shows the time-dependent gaseous concentrations of the components NO_x, NO, NO_2, N_2O, SO_2, and O_2 when plasma is generated for a medium water-film flow rate of 100 mL/min. The measurements for particle collection shown in **Fig. 6(b)** and gaseous components as shown in **Fig. 9** are performed simultaneously. As shown in **Fig. 9(a)**, NO decreases from 95 ppm to 0 ppm, NO_x decreases from 97 ppm to 2 ppm, and SO_2 decreases from 88 ppm to 0 ppm when the applied voltage is 31 kV and discharge power is 32 W. The system achieves NO_x removal efficiency of 98% or higher and SO_x removal efficiency of 100%. As shown in **Fig. 9(b)**, NO decreases from 97 ppm to 0 ppm, NO_x decreases from 99 ppm to 6 ppm, and SO_2 decreases from 97 ppm to 0 ppm when the applied voltage is 27 kV and discharge power is 12 W. The system achieves NO_x removal efficiency of 86% or higher and SO_x removal efficiency of 100%. As shown in **Fig. 9(c)**, NO decreases from 97 ppm to 0 ppm, NO_x decreases from 99 ppm to 21 ppm, and SO_2 decreases from 90 ppm to 3 ppm when the applied voltage is 26 kV and discharge power is 12 W. Consequently, the system achieves NO_x removal efficiency of 78% or higher and SO_x removal efficiency of 97% or higher. At q = 100 mL/min, the NO_x removal efficiency increases with increase the applied voltage or the discharge power. In **Fig. 9(a)–(c)**, N_2O concentrations are less than 7 ppm in all cases, which is much lower than that of the removed NO_x.

Fig. 10 shows the time-dependent concentrations of the gas components NO_x, NO, NO_2, N_2O, SO_2, and O_2 when plasma is generated for a lower water-film flow rate of 50 mL/min. The measurements for the particle collection shown in **Fig. 6(c)** and gaseous components as shown in **Fig. 10** are performed simultaneously. As shown in **Fig. 10(a)**, NO decreases from 96 ppm to 0 ppm, NO_x decreases from 98 ppm to 4 ppm, and SO_2 decreases from 93 ppm to 2 ppm when the applied voltage is 32 kV and discharge power is 31 W. Consequently, the system achieves NO_x removal efficiency of 93% or higher and SO_x removal efficiency of 98% or higher. As shown in **Fig. 10(b)**, NO decreases from 95 ppm to 0 ppm, NO_x decreases from 97 ppm to 13 ppm, and SO_2 decreases from 98 ppm to 3 ppm when the applied voltage is 30 kV and discharge power is 19 W. Thus, the system achieves NO_x removal efficiency of 84% or higher and SO_x removal efficiency of 96% or higher. NO_x removal efficiency becomes lower than those at V = 29 and 32 kV because the variation of the discharge power was large, 25% in maximum during the experiment. As shown in **Fig. 10(c)**, NO decreases from 98 ppm to 0 ppm, NO_x decreases from 99 ppm to 11 ppm, and SO_2 decreases from 92 ppm to 3 ppm when the applied voltage is 29 kV and discharge power is 17 W. Consequently, the system achieves NO_x removal efficiency of 89% or higher and SO_x removal efficiency of 94% or higher. In **Fig. 10(a)–(c)**, the N_2O concentrations are less than 13 ppm in all cases, which is much lower than that of the removed NO_x. The O_2 concentration is 10–12% in these experiments, as seen in **Figs. 8–10**. This concentration range is set to be equivalent to the concentration in the combustion exhaust gas, such as that by a diesel engine.

As a result of measuring the temperature of the ground electrode wall for 15 minutes under the discharge at q = 50, 100, and 200 mL/min, the temperature increased by up to 3°C from 19°C to 22°C under all flow rate conditions. However, the temperature was

stable because the heat is removed by the water film. Therefore, the proposed technology is capable of treating NO_x at low temperatures.

Characteristics of Solution

Fig. 11 shows the results for the time variations of nitrate ion (NO_3^-) and nitrite ion (NO_2^-) concentrations in the water film. The voltage V and flow rate q are varied. In all conditions, NO_3^- and NO_2^- are initially detected at t = –10 min owing to the slight dissolution of NO_3^- and NO_2^- in distilled water. As shown in **Fig 11(a)–(c)**, the NO_3^- concentrations increase during the air plasma process. However, the increase rate of NO_2^- is much lower than that of NO_3^-; the reason for this is considered to be the ability of self-decomposition of NO_2^-. Further, as the flow rate of the water film increases, the NO_3^- concentrations increase slightly; this is attributable to the increases in current and discharge power as the flow rate of water increases, thus shifting the reaction from the gas phase to the liquid phase.

Fig. 12 shows the pH and conductivity of the water film. In **Fig. 12(b)**, the pH of the initial distilled water ranges from 4 to 7 for q = 100 mL/min. During the water film circulation, SO_2 is absorbed, which decreases the pH and increases conductivity. For three applied voltage conditions, the pH decreases and conductivity increases at t = 10 min owing to the absorption of SO_2, NO_2, HNO_2, and HNO_3. These trends in the pH and conductivity of the water film are also similar for other water-film flow rates, as shown in **Fig. 12(a)** and **(b)**.

Effect of PM collection on energy yield for NO_x removal

Next, the removal energy efficiency or energy yield for NO_x removal is considered based on the results in **Figs. 7–9**. It is observed that NTP has little effect on the energy yield for SO_x removal. Therefore, it is enough to evaluate the energy yield for NO_x removal. To identify the effect of PM precipitation or collection on the energy yield for NO_x removal, the simultaneous PM removal performance in the present study is compared with a previous report for energy yield. The energy yield is calculated by the following equation [24]:

$$\eta_{NO_x} = [(\Delta NO) + (\Delta NO_2)] \times 10^{-6} \times M_{NO_2} \times \frac{pQ}{RT} \times \frac{1}{P} \times 60 \quad (9)$$

where ΔNO and ΔNO_2 are the removed NO and NO_2 concentrations (ppm), M_{NO_2} is the molecular mass of NO_2 (g/mol), p is the pressure (kPa), Q is the gas flow rate (L/min), R is the gas constant (kPa/(mol·K)), T is the temperature (K), and P is the discharge power (W).

Fig. 13 shows the energy yield of NO_2, which has the unit g(NO_2)/kWh, against specific energy (SE), which is measured in units of (Wh/m^3). The compared data are from experiments conducted under the following conditions: air plasma treatment, gas flow rate of 4 L/min, and initial NO and SO_2 concentrations of about 100 ppm each. In the previous report [24], the experimental data for NO_x and SO_x treatment with PM were obtained under the same conditions as the present experiments. The experimental data for NO_x and SO_x treatment without PM were given in another study [25]. It is observed from **Fig. 13** that the energy yield for NO_2 removal is almost inversely proportional to SE, as seen from the solid curve, because the average NO_x removal efficiency is high and more

than 80%. It is seen from the graph that the present results are similar to those reported previously [24], which included the particles quantitatively. Further, the previous data [25] that did not consider the particles showed similar results. Moreover, the results in the present and previous [24] studies show that the average collection efficiency is more than 95% in the 22–334 nm particle size range with simultaneous removal of NO_x and SO_x. Therefore, it can be concluded that the electrostatic PM precipitation has little effect on the removal of NO_x and SO_x in the simultaneous removal because the energy required for electrostatic PM precipitation is lower.

From the aforementioned results, it is obvious that the wet-type NTP reactor can simultaneously remove NO_x, SO_x, and nanoparticles. Actual exhaust gas, such as diesel one, has various PM components and concentrations of NO_x and SO_x, so it is necessary to study actual exhaust gas treatment with actual diesel engines in order to put this technology to practical use in the future. All the physical and chemical interactions will vary in real industry. These experiments were conducted on the laboratory scale with a gas flow rate of 4 L/min; however, it is expected that treatment of large flow rates of exhaust gases, including NO_x, SO_x, and nanoparticles, can be achieved under practical scenarios by the parallel arrangement of the multiple wet-type NTP reactors. The arrangement could enable simultaneous removal of PM, NO_x, and SO_x with larger flow rate and high efficiency of over 90%, which is confirmed from the result of this study.

Conclusions

In this study, we conducted laboratory-scale experiments for the simultaneous removal of PM, NO_x, and SO_x using the wet-type NTP reactor without any chemical agents. Furthermore, we obtained the partial collection efficiency for nanoparticles by measuring the particle number concentration using the SMPS. In the experiments, we collected 98% of the particles with diameters in the range of 22–334 nm at an applied voltage of 28 kV when the gas flow rate, frequency of high-voltage pulse, and solution flow rate were 4 L/min, 210 Hz, and 200 mL/min, respectively. The water film flow rate had no effect on the particle collection efficiency in the 50–200 mL/min flow rate range because the SO_x was sufficiently absorbed by the water film, and electrical conductivity of water was increased to stabilize the electrical discharge. Further, the simultaneous removal of 92% of NO_x and 98% of SO_2 was achieved at an applied voltage of 28 kV for a gas flow rate, frequency of high-voltage pulse, and solution flow rate of 4 L/min, 210 Hz, and 200 mL/min, respectively. The electrostatic PM precipitation has little effect on the removal of NO_x and SO_x in the simultaneous removal because the energy required for electrostatic PM precipitation is lower. Based on these results, we demonstrated the feasibility of simultaneous removal of PM, NO_x, and SO_x. For industrial applications, several of the proposed plasma reactors should be placed in parallel and tested for a real-sizes system.

Acknowledgments

The authors thank Mr. K. Kishimoto, who is a graduate student at Osaka Prefecture University, for carrying out the experiments.

Funding

The work was supported in part by a research collaboration fund of Samsung Advanced

Institute of Technology (SAIT).

Conflict of interest

The author declares that they have no conflict of interest.

References

[1] A. S. Ansari and A. N. Pandis, "Response of inorganic PM to precursor concentrations", *Environ. Sci. Technol*. 32, pp. 2706–2714, 1998.

[2] J. J. West, A. S. Ansari, and S. N. Pandis, "Marginal $PM_{2.5}$: Nonlinear aerosol mass response to sulfate reductions in the eastern united states", J. Air Waste Manage. Assoc., 49, pp. 1415–1424, 1999.

[3] P. Forzatti, "Present status and perspectives in de-NO_x SCR catalysis", Appl. Catal., A, 222, pp. 221–236, 2001.

[4] D. Damma, P. R. Ettireddy, B. M. Reddy, and P. G. Smirniotis, "A review of low temperature NH3-SCR for removal NOx", *Catalysts*, 9(4), 349, 2019.

[5] B. Wang, Z. Pan, Z. Du, H. Cheng, and F. Cheng, "Effect of impure components in flue gas desulfurization (FGD) gypsum on the generation of polymorph $CaCO_3$ during carbonation reaction," *J. Hazard. Mater.*, 369, pp.236–243, 2019.

[6] J. G. Majeed, B. Korda, and E. Békássy-Molnár, "Comparison of the efficiencies of sulfur dioxide absorption using calcium carbonate slurry and sodium hydroxide solution in an ALT reactor," *Gas Sep. Purif.*, 9, 2, pp.111–120, 1995.

[7] Yang, B., Shen, Y., Shen, S. and Zhu, S., Regeneration of the deactivated TiO_2-ZrO_2-CeO_2/ATS catalyst for NH_3-SCR of NO_x in glass furnace, *J. Rare Earths*, 31, 2, pp.130–136, 2013.

[8] J. V. Caneghem, J. D. Greef, C. Block, and C. Vandecasteele, "NO_x reduction in waste incinerators by selective catalytic reduction (SCR) instead of selective non catalytic reduction (SNCR) compared from a life cycle perspective: a case study", *J. Clean. Prod.*, 17, pp. 4452–4460, 2016.

[9] B. Han, H. J. Kim, and Y. J. Kim, "Removal of NO and SO_2 in a cylindrical film pulse corona discharge", *IEEE Trans. Ind. App.*, 51, 1, pp. 679–684, 2015.

[10] S. Kanazawa, J. S. Chang, G. F. Round, G. Sheng, T. Ohkubo, Y. Nomoto, and T. Adachi, "Removal of NO_x from flue gas by corona discharge activated methane radical shower," *J. Electrost.*, 40–41, pp.651–656, 1997.

[11] X. Zhu, C. Zheng, X. Gao, X. Shen, Z. Wang, Z. Luo, and K. Cen, "Experimental study of NO_2 reduction in N_2/Ar and O_2/Ar mixtures by pulsed corona discharge," *J. Environ. Sci.*, 26, pp.2249–2256, 2014.

[12] K. Okazaki, A. Mizuno, K. Shimizu, and T. Niwa, "Application of semi-wet type corona discharge reactor to the simultaneous removal of NO_x, SO_x, and fly ash in pulverized coal combustion," *Proc. JSME-ASME Int. Conf. on Power Eng.,* 2, pp.103–108, 1993.

[13] H. H. Kim, C. Wu, Y. Kinoshita, K. Takashima, S. Katsura, and A. Mizuno, "The influence of reaction conditions on SO_2 oxidation in a discharge plasma reactor," *IEEE Trans. Ind. Appl.,* 37, 2, pp.480–486, 2001.

[14] H. J. Kim, A. Han, and Y. J. Kim, "NO_x removal performance of a wet reduction scrubber combined with oxidation by an indirect DBD plasma for semiconductor manufacturing industries", *IEEE Trans. Ind. App.*, 54, pp. 6401–6407, 2018

[15] T. Wang and B. Sun, "Effect of temperature and relative humidity on NO_x removal by dielectric barrier discharge with acetylene," *J. Fuel Process. Technol.,* 144, pp.1309–114, 2016.

[16] I. Nagao, M. Nishida, K. Yukimura, S. Kambara, and T. Maruyama, "NO_x removal using nitrogen gas activated by dielectric barrier discharge at atmospheric pressure," *Vacuum,* 65, pp.481–487, 2002.
[17] J. Zhang, R. Zhang, X. Chen, M. Tong, W. Kang, S. Guo, Y. Zhou, and J. Lu, "Simultaneous removal of NO and SO_2 from flue gas by ozone oxidation and NaOH absorption," *Ind. Eng. Chem. Res.*, 53, pp.6450−6456, 2014.
[18] T. Yamamoto, C. L. Yang, R. Michael, and Z. Kravets, "Plasma-assisted chemical process for NO_x control," *IEEE Trans. Ind. Appl.*, 36, 3, pp.923–927, 2000.
[19] Y. S. Mok, "Combined desulphurization and denitrification using dielectric barrier discharge and wet reduction technique," *J. Chem. Eng. Jpn.*, 39, 3, pp.366–372, 2006.
[20] D. Xie, Y. Sun, T. Zhu, and L. Ding, "Removal of NO in mist by the combination of plasma oxidation and chemical absorption," *Energ. Fuel.,* 30, pp.5071–5076, 2016.
[21] M. B. Chang, H. M. Lee, F. Wu, and C. R. Lai, "Simultaneous removal of Nitrogen oxide/nitrogen dioxide/sulfur dioxide from gas streams by combined plasma scrubbing technology", J. Air Waste Manage. Assoc., 54, pp. 941–949, 2004.
[22] T. Kuroki, M. Takahashi, M. Okubo, and T. Yamamoto, "Single-stage plasma-chemical process for particulates, NO_x, and SO_x simultaneous removal," *IEEE Trans. Ind. Appl.*, 38, 5, pp.1204–1209, 2002.
[23] T. Kuroki, S. Nishii, T. Kuwahara, and M. Okubo, "Nanoparticle removal and exhaust gas cleaning using gas-liquid interfacial nonthermal plasma," *J. Electrost.,* 87, pp.86–92, 2017.
[24] T. Takehana, T. Kuroki and M. Okubo, "Evaluation on nitrogen oxides and nanoparticle removal and nitrogen monoxide generation using a wet-type nonthermal plasma reactor," *J. Phys. D: Appl. Phys.,* 51, 204002, 2018.
[25] T. Kuroki, S. Nomura, H. Yamasaki, and M. Okubo, "Performance of a wet-type nonthermal plasma reactor for NO_x, SO_x, and wastewater treatment," *Proc. IEEE Ind. Appl. Soc. Annual Meeting*, 2019, pp.1–5.
[26] S. Zhou, J. Zhou, Y. Feng, and Y. Zhu, "Marine emission pollution abatement using ozone oxidation by a wet scrubbing method", *Ind. Eng. Chem. Res.,* 55, 20, pp. 5825–5831, 2016.
[27] C. J. Yu, F. Xu, Z. Y. Luo, W. Cao, B. Wei, X. Gao, M. X. Fang, and K. F. Cen, "Influences of water vapor and fly ash addition on NO and SO_2 gas conversion efficiencies enhanced by pulsed corona discharge", *J. Electrostat.*, 67, 6, pp. 829–834, 2009.

Figure and Table captions

Fig. 1 Schematic of the wet-type plasma reactor.

Fig. 2 Experimental setup for simultaneous PM, NO, and SO_x removal.

Fig. 3 Waveforms of the voltage v (kV), current i (A), and instantaneous power (VA) (V = 28 kV, q = 200 mL/min, average discharge power = 31 W).

Fig. 4 Relationship between discharge power and applied peak voltage for various flow rates.

Fig. 5 Particle size distribution of nanoparticles.

Fig. 6 Partial collection efficiencies for nanoparticles for various flow rates of the water film with frequency f = 210 Hz, gas flow rate Q = 4 L/min, and L = 260 mm: (a) q = 200 mL/min, (b) q = 100 mL/min, and (c) q = 50 mL/min.

Fig. 7 Partial collection efficiencies for particles with specified diameters in the present work and a previous study [23].

Fig. 8 Gaseous concentrations at the outlet of the reactor for various applied peak voltages with frequency, gas flow rate, and water flow rate of 210 Hz, 4 L/min, and 200 mL/min, respectively, for L = 260 mm: (a) V = 28 kV, (b) V = 27 kV, and (c) V = 26 kV.

Fig. 9 Gaseous concentrations at the outlet of the reactor for various applied peak voltages with frequency, gas flow rate, and water flow rate of 210 Hz, 4 L/min, and 100 mL/min, respectively, for L = 260 mm: (a) V = 31 kV, (b) V = 27 kV, and (c) V = 26 kV.

Fig. 10 Gaseous concentrations at the outlet of the reactor for various applied peak voltages with frequency, gas flow rate, and water flow rate of 210 Hz, 4 L/min, and 50 mL/min, respectively, for L = 260 mm: (a) V = 32 kV, (b) V = 30 kV, and (c) V = 29 kV.

Fig. 11 Nitrate and nitrite ion concentrations in water for various flow rates of the water film q with frequency and gas flow rate of 210 Hz and 4 L/min, respectively: (a) q = 200 mL/min, (b) q = 100 mL/min, and (c) q = 50 mL/min.

Fig. 12 pH and conductivity of the water film for various flow rates of the liquid film q with frequency and gas flow rate of 210 Hz and 4 L/min, respectively: (a) q = 200 mL/min, (b) q = 100 mL/min, and (c) q = 50 mL/min.

Table 1 Relationships between energy yields for NO_2 reduction and discharge power for the present work and previous studies [24], [25].

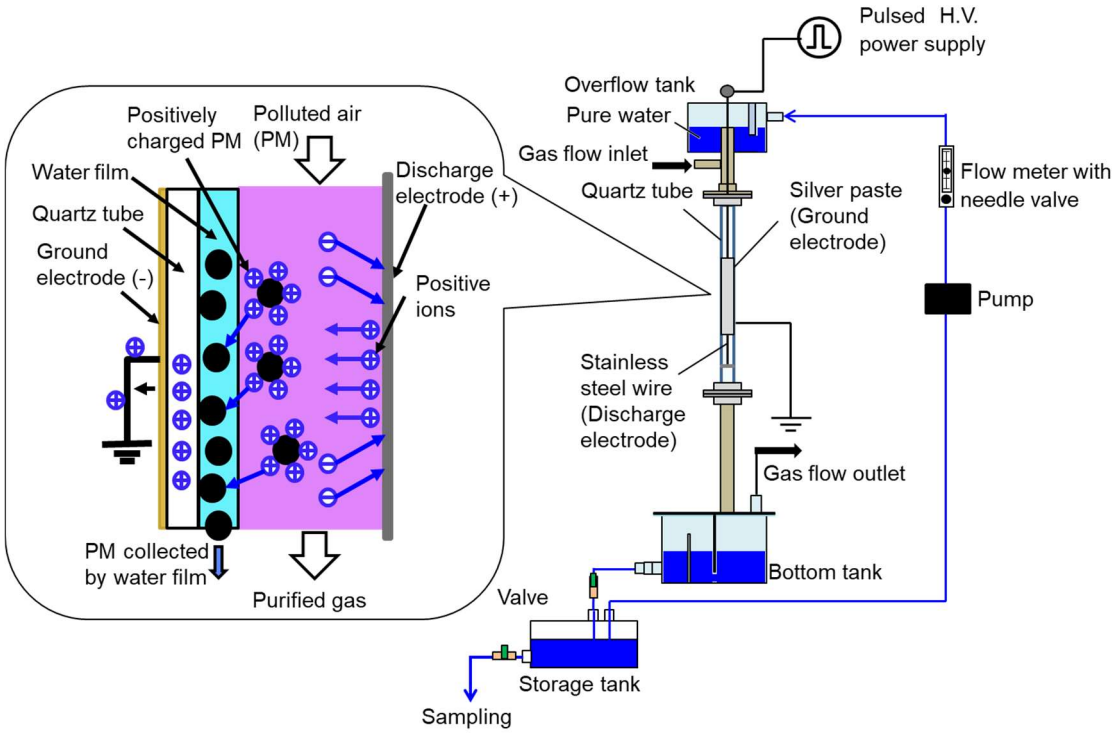
Positively charged PM
Polluted air (PM)
Water film
Quartz tube
Ground electrode (-)
Discharge electrode (+)
Positive ions
PM collected by water film
Purified gas
Pulsed H.V. power supply
Overflow tank
Pure water
Gas flow inlet
Quartz tube
Silver paste (Ground electrode)
Flow meter with needle valve
Pump
Stainless steel wire (Discharge electrode)
Gas flow outlet
Bottom tank
Valve
Storage tank
Sampling

Fig. 1

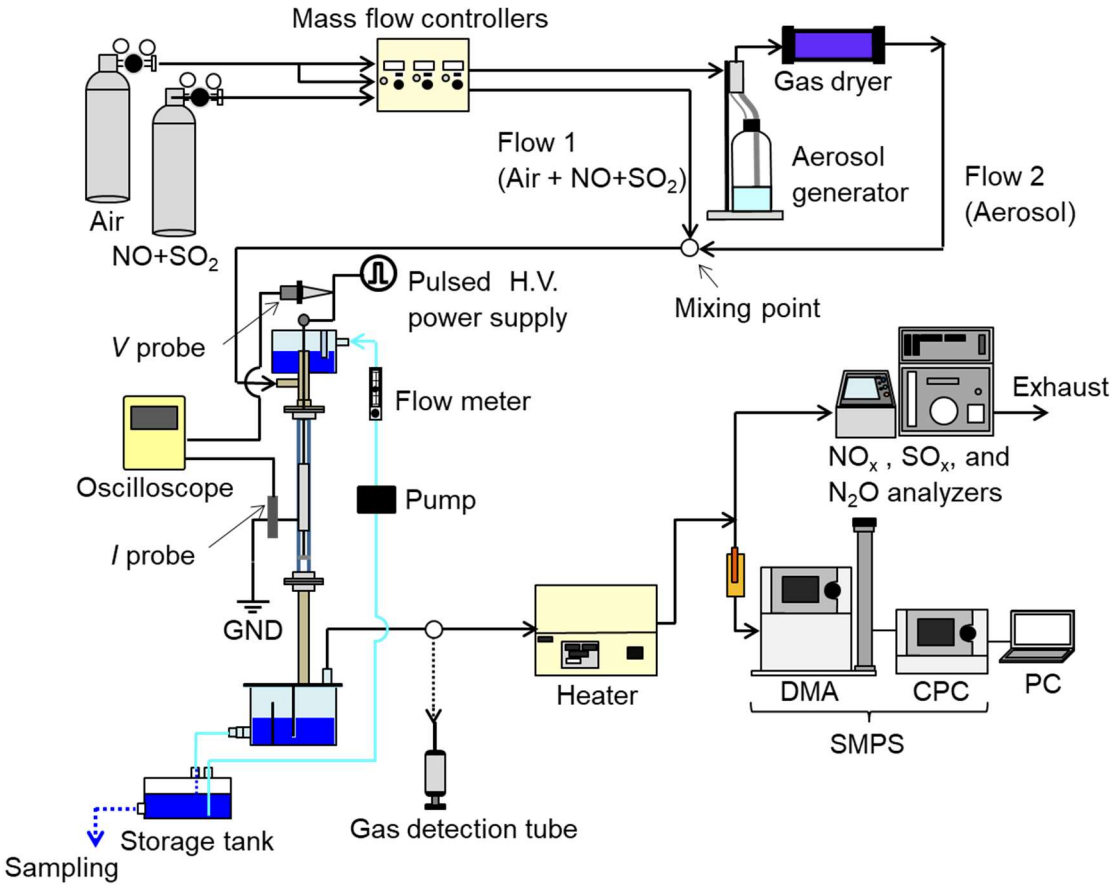
Mass flow controllers
Gas dryer
Flow 1
(Air + NO+SO2)
Aerosol
generator
Flow 2
(Aerosol)
Air
NO+SO2
Pulsed H.V.
power supply
Mixing point
V probe
Flow meter
Exhaust
NOx , SOx, and
N2O analyzers
Oscilloscope
Pump
I probe
GND
Heater
DMA
CPC
PC
SMPS
Storage tank
Sampling
Gas detection tube

Fig. 2

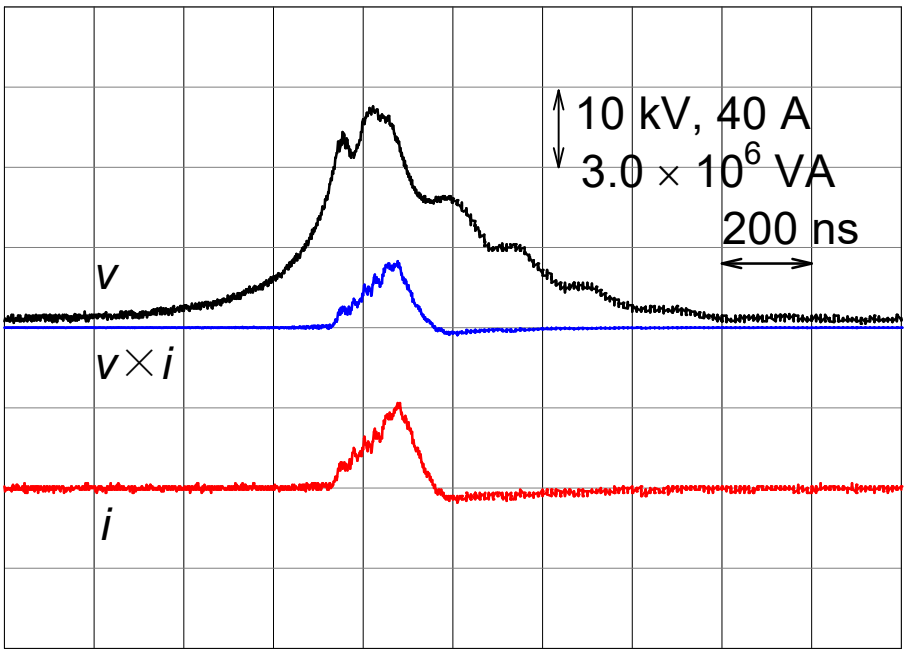

Fig. 3

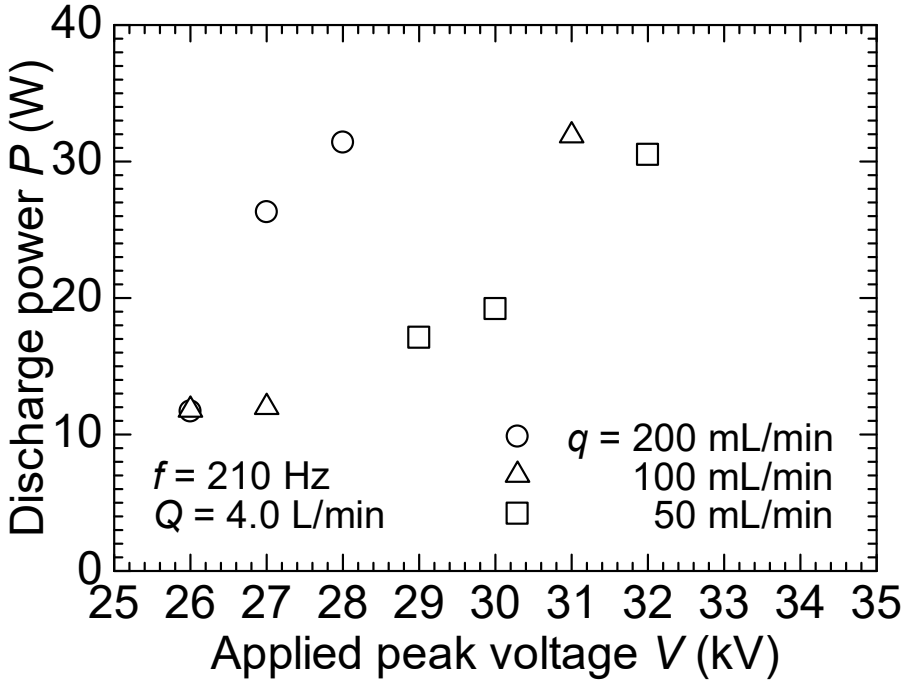
Discharge power P (W)
Applied peak voltage V (kV)
f = 210 Hz
Q = 4.0 L/min
q = 200 mL/min
100 mL/min
50 mL/min
0
10
20
30
40
25
26
27
28
29
30
31
32
33
34
35

Fig. 4

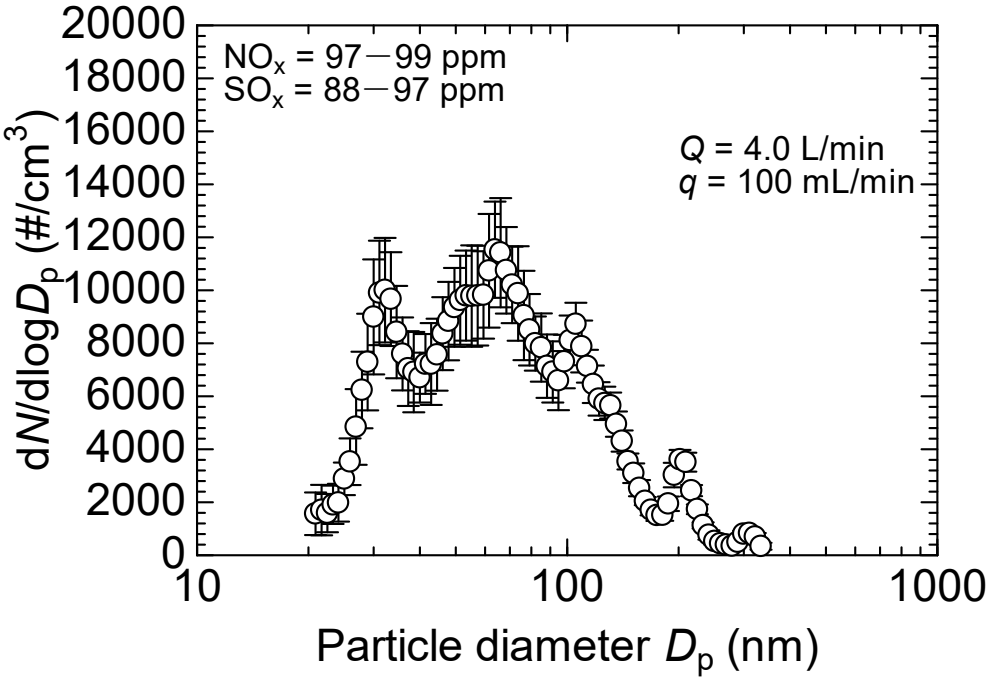
20000
18000
16000
14000
12000
10000
8000
6000
4000
2000
0
10
100
1000
NOx = 97—99 ppm
SOx = 88—97 ppm
Q = 4.0 L/min
q = 100 mL/min
dN/dlogDp (#/cm3)
Particle diameter Dp (nm)

Fig. 5

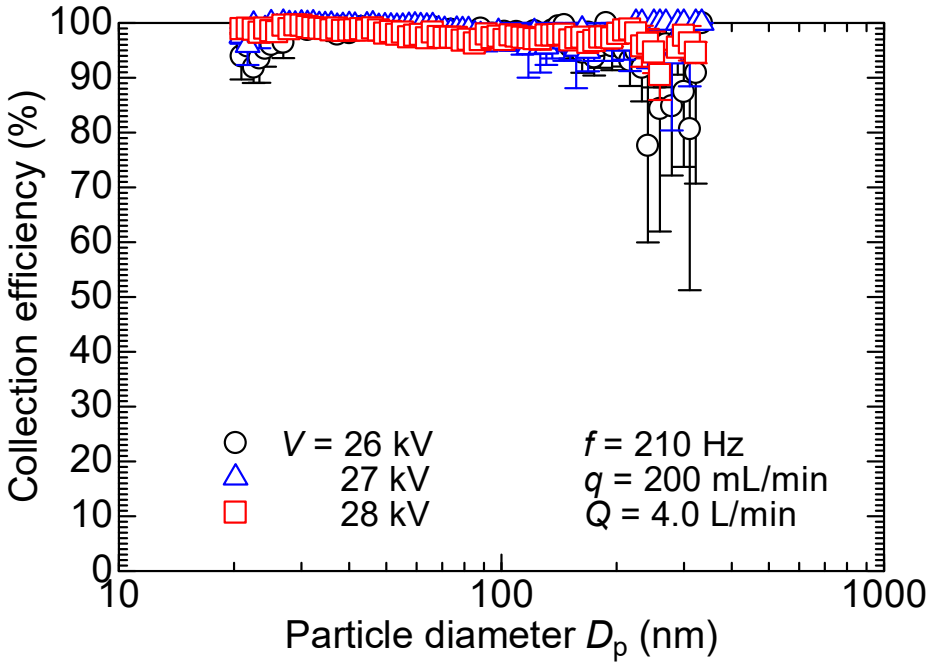
Collection efficiency (%)
Particle diameter D_p (nm)
V = 26 kV
27 kV
28 kV
f = 210 Hz
q = 200 mL/min
Q = 4.0 L/min

(a)

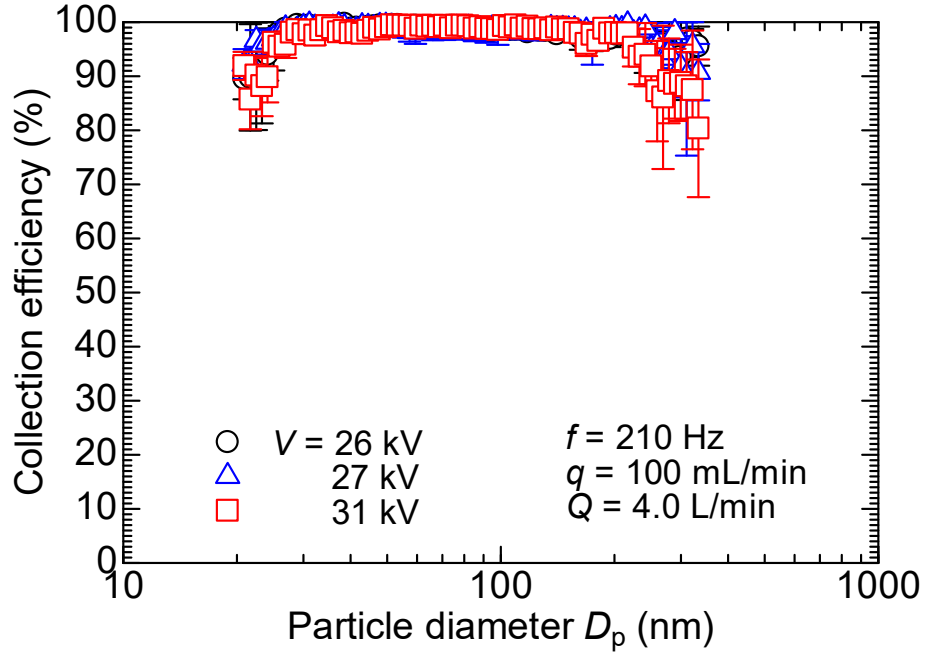
Collection efficiency (%)
Particle diameter D_p (nm)
V = 26 kV
27 kV
31 kV
f = 210 Hz
q = 100 mL/min
Q = 4.0 L/min

(b)

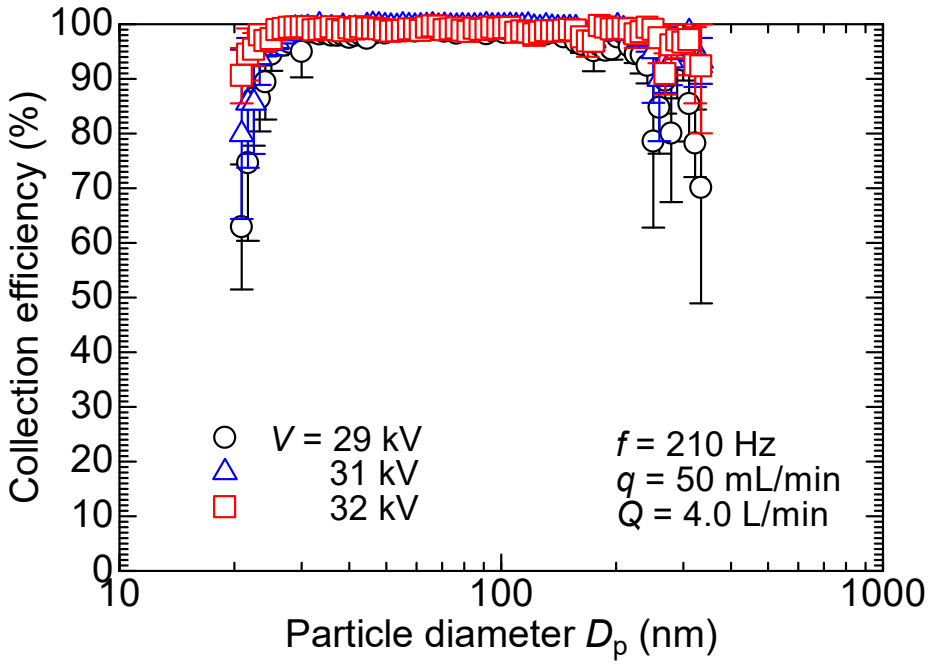
Collection efficiency (%)
100
90
80
70
60
50
40
30
20
10
0
10
100
1000
Particle diameter D_p (nm)
V = 29 kV
31 kV
32 kV
f = 210 Hz
q = 50 mL/min
Q = 4.0 L/min

(c)

Fig. 6

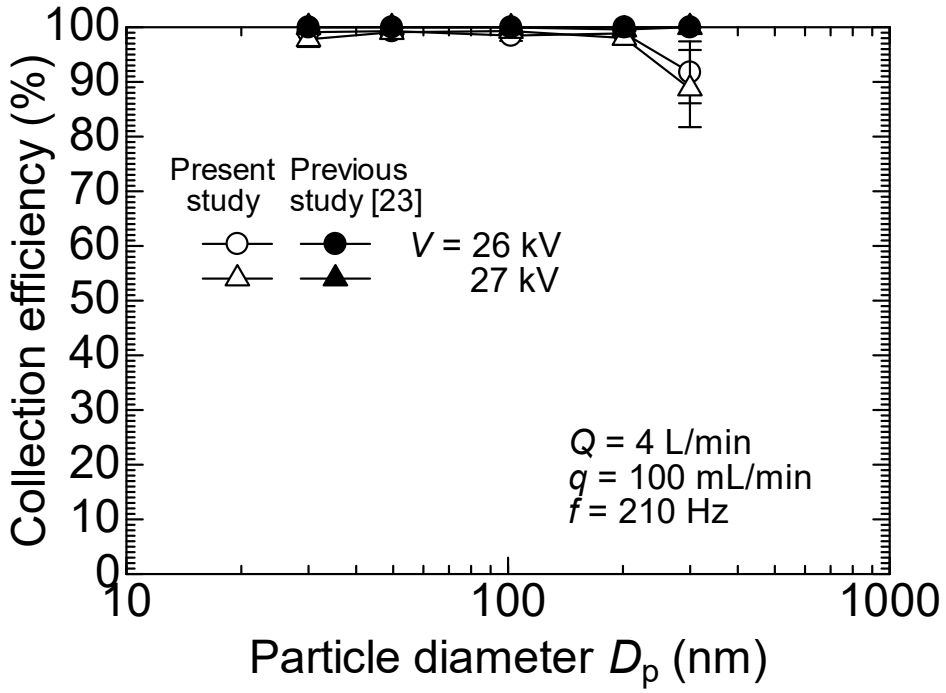
Collection efficiency (%)
100
90
80
70
60
50
40
30
20
10
0
10
100
1000
Particle diameter D_p (nm)
Present study
Previous study [23]
V = 26 kV
27 kV
Q = 4 L/min
q = 100 mL/min
f = 210 Hz

Fig. 7

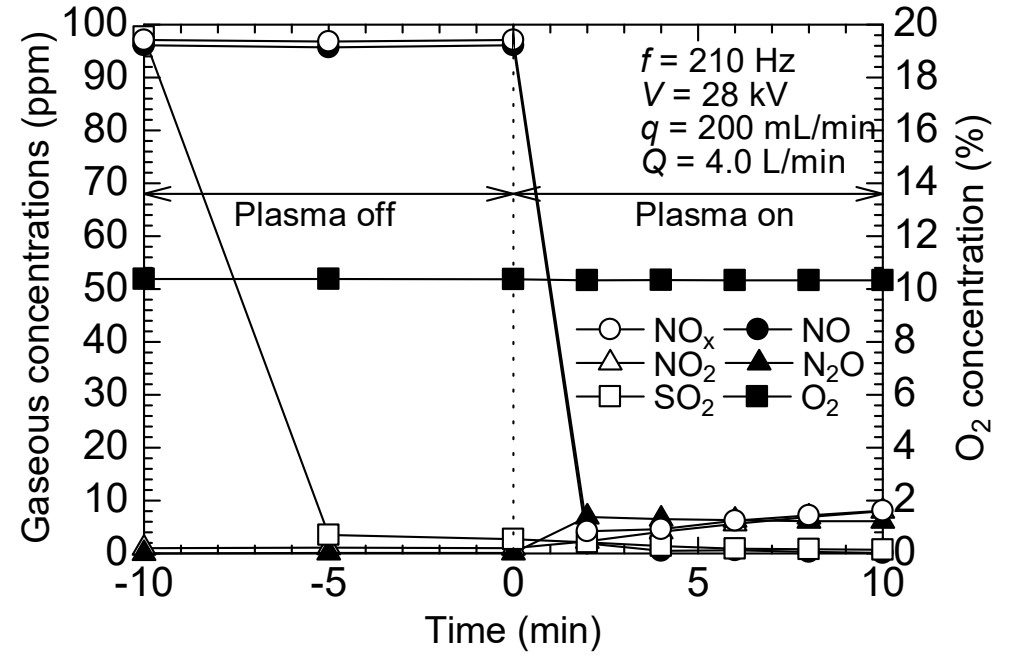
f = 210 Hz
V = 28 kV
q = 200 mL/min
Q = 4.0 L/min
Plasma off
Plasma on
NOx
NO
NO2
N2O
SO2
O2
Gaseous concentrations (ppm)
O2 concentration (%)
Time (min)

(a)

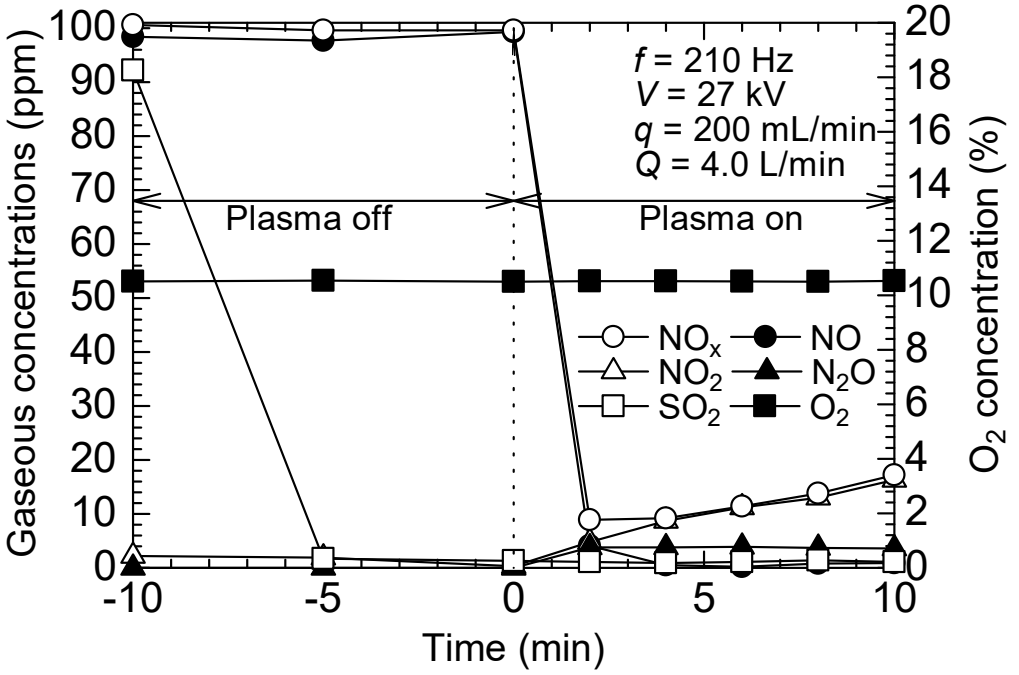
f = 210 Hz
V = 27 kV
q = 200 mL/min
Q = 4.0 L/min
Plasma off
Plasma on
NOx
NO
NO2
N2O
SO2
O2
Gaseous concentrations (ppm)
O2 concentration (%)
Time (min)

(b)

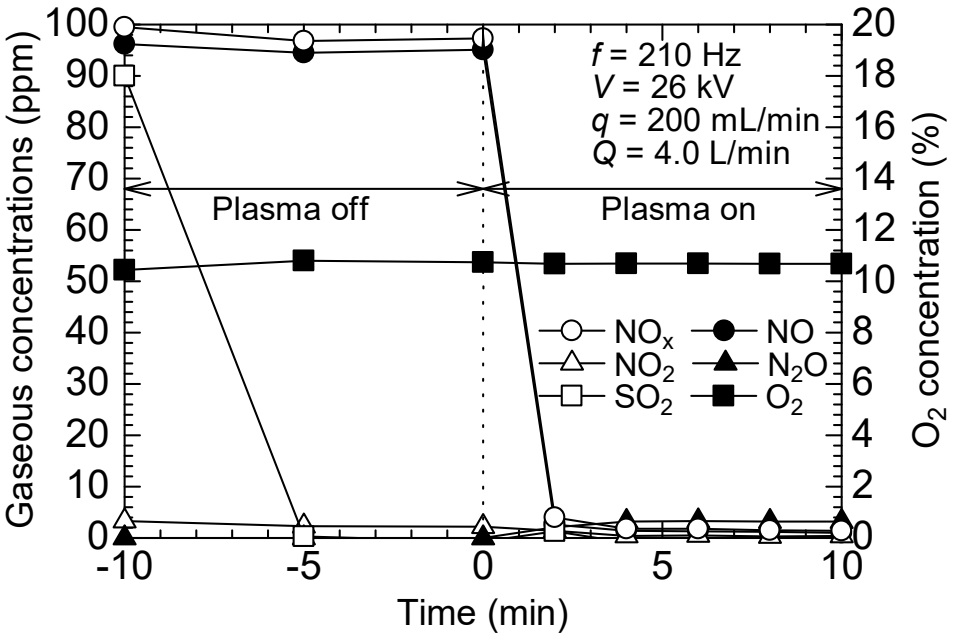
Gaseous concentrations (ppm)
O2 concentration (%)
Time (min)
f = 210 Hz
V = 26 kV
q = 200 mL/min
Q = 4.0 L/min
Plasma off
Plasma on
NOx
NO
NO2
N2O
SO2
O2

(c)

Fig. 8

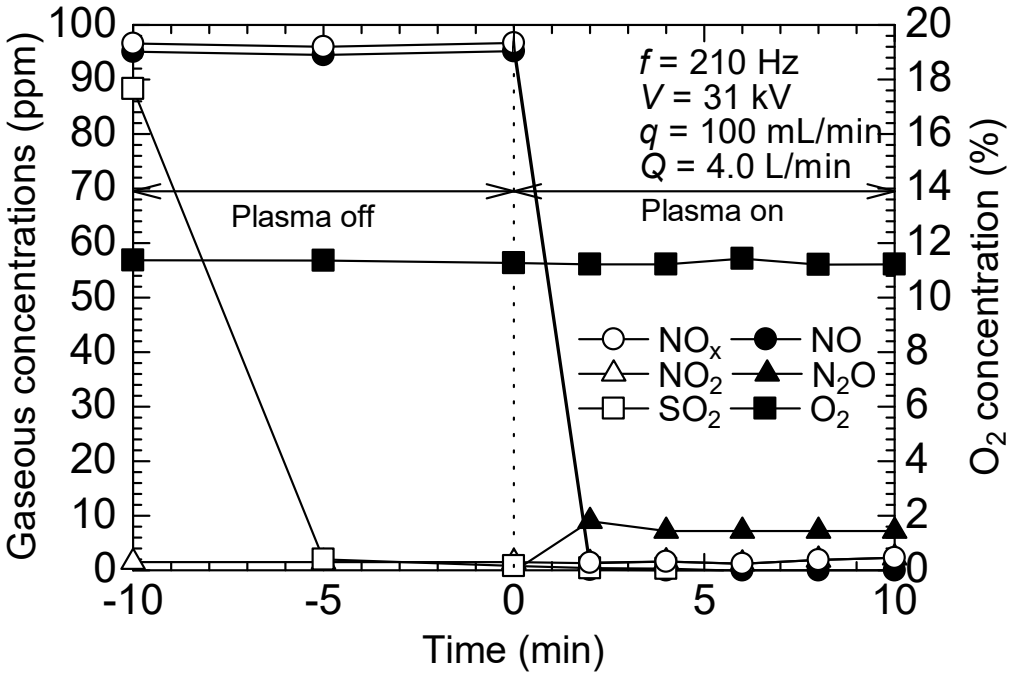
f = 210 Hz
V = 31 kV
q = 100 mL/min
Q = 4.0 L/min
Plasma off
Plasma on
NOx
NO
NO2
N2O
SO2
O2
Gaseous concentrations (ppm)
O2 concentration (%)
Time (min)

(a)

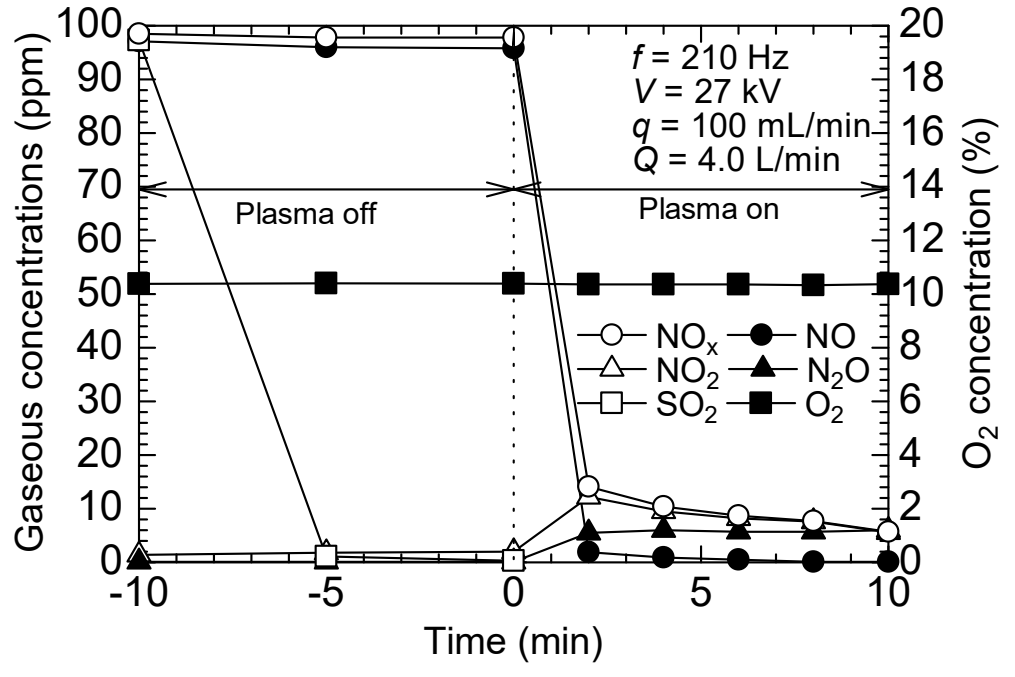
f = 210 Hz
V = 27 kV
q = 100 mL/min
Q = 4.0 L/min
Plasma off
Plasma on
NOx
NO
NO2
N2O
SO2
O2
Gaseous concentrations (ppm)
O2 concentration (%)
Time (min)

(b)

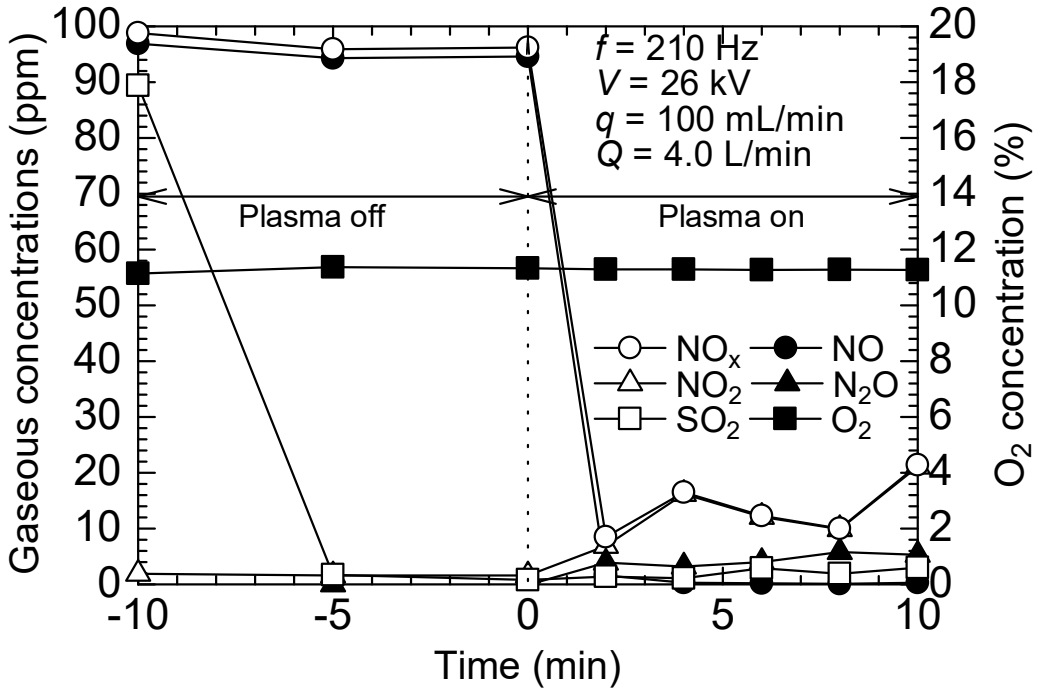
f = 210 Hz
V = 26 kV
q = 100 mL/min
Q = 4.0 L/min
Plasma off
Plasma on
NOx
NO
NO2
N2O
SO2
O2
Gaseous concentrations (ppm)
O2 concentration (%)
Time (min)
100
90
80
70
60
50
40
30
20
10
0
20
18
16
14
12
10
8
6
4
2
0
-10
-5
0
5
10

(c)

Fig. 9

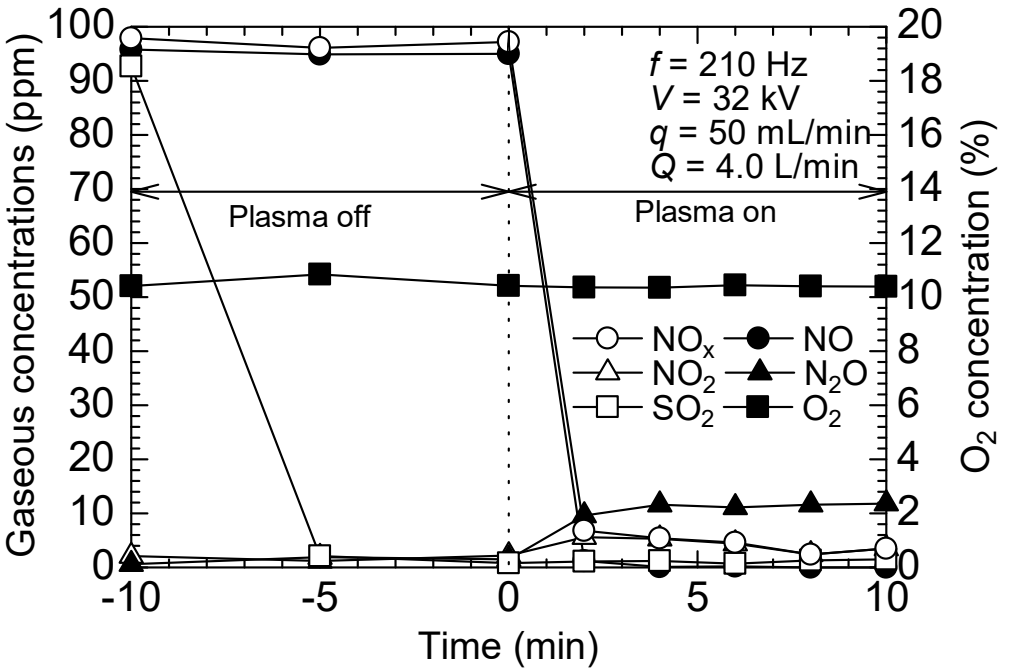
f = 210 Hz
V = 32 kV
q = 50 mL/min
Q = 4.0 L/min
Plasma off
Plasma on
NOx
NO
NO2
N2O
SO2
O2
Gaseous concentrations (ppm)
O2 concentration (%)
Time (min)

(a)

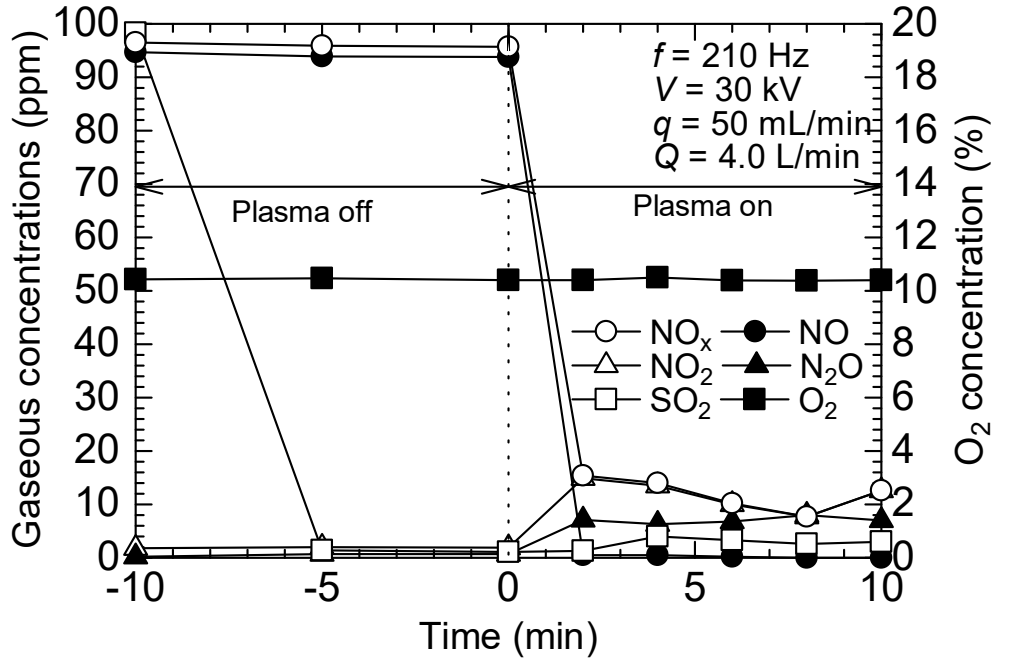
f = 210 Hz
V = 30 kV
q = 50 mL/min
Q = 4.0 L/min
Plasma off
Plasma on
NOx
NO
NO2
N2O
SO2
O2
Gaseous concentrations (ppm)
O2 concentration (%)
Time (min)

(b)

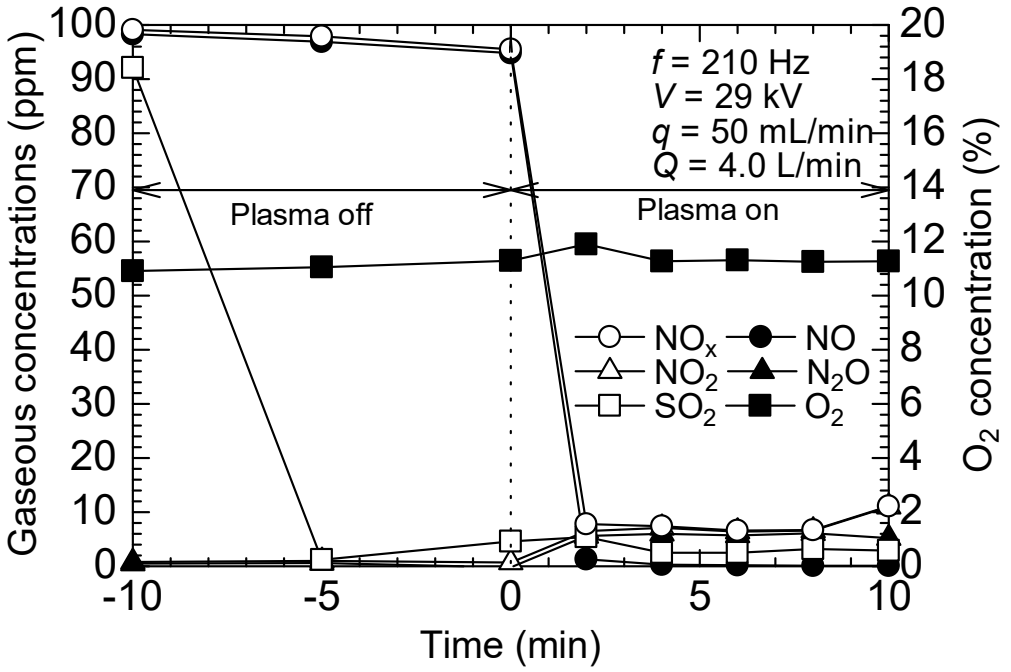
Gaseous concentrations (ppm)
O2 concentration (%)
Time (min)
f = 210 Hz
V = 29 kV
q = 50 mL/min
Q = 4.0 L/min
Plasma off
Plasma on
NOx
NO
NO2
N2O
SO2
O2

(c)

Fig. 10

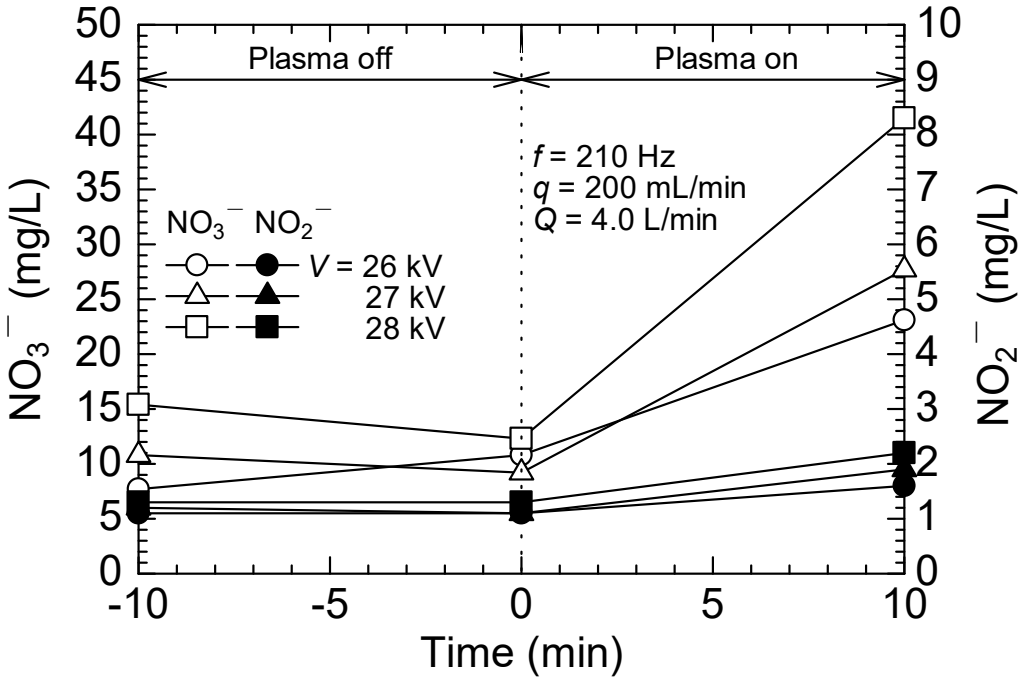
Plasma off
Plasma on
f = 210 Hz
q = 200 mL/min
Q = 4.0 L/min
NO3− NO2−
V = 26 kV
27 kV
28 kV
NO3− (mg/L)
NO2− (mg/L)
Time (min)

(a)

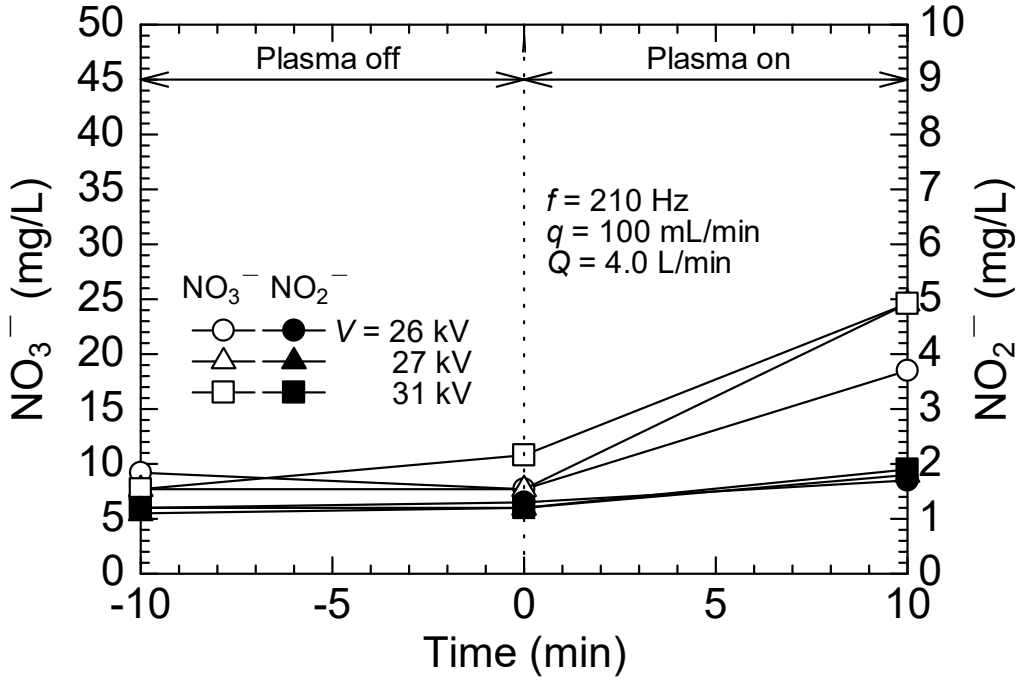
Plasma off
Plasma on
f = 210 Hz
q = 100 mL/min
Q = 4.0 L/min
NO3− NO2−
V = 26 kV
27 kV
31 kV
NO3− (mg/L)
NO2− (mg/L)
Time (min)

(b)

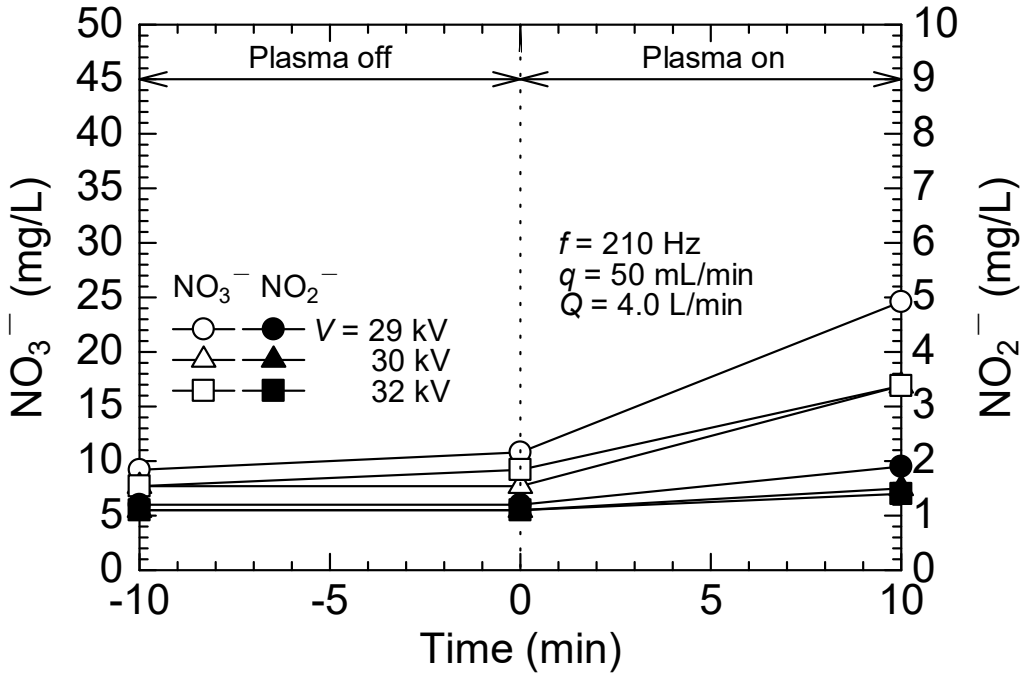
Plasma off
Plasma on
NO_3^- NO_2^-
V = 29 kV
30 kV
32 kV
f = 210 Hz
q = 50 mL/min
Q = 4.0 L/min
NO_3^- (mg/L)
NO_2^- (mg/L)
Time (min)
50
45
40
35
30
25
20
15
10
5
0
10
9
8
7
6
5
4
3
2
1
0
-10
-5
0
5
10

(c)

Fig. 11

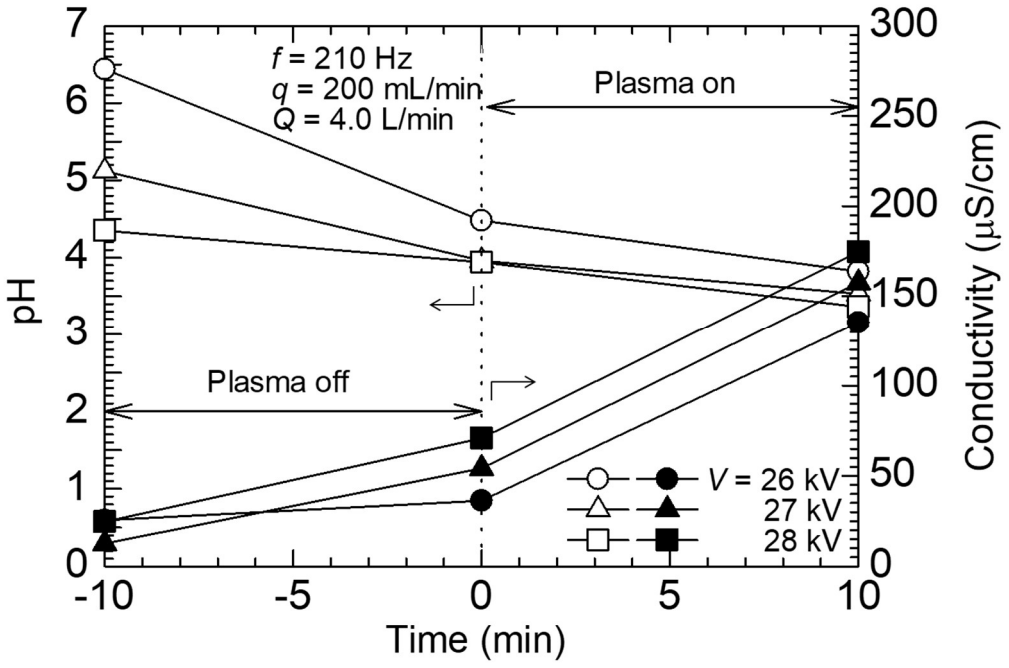
f = 210 Hz
q = 200 mL/min
Q = 4.0 L/min
Plasma on
Plasma off
V = 26 kV
27 kV
28 kV
pH
Conductivity (μS/cm)
Time (min)

(a)

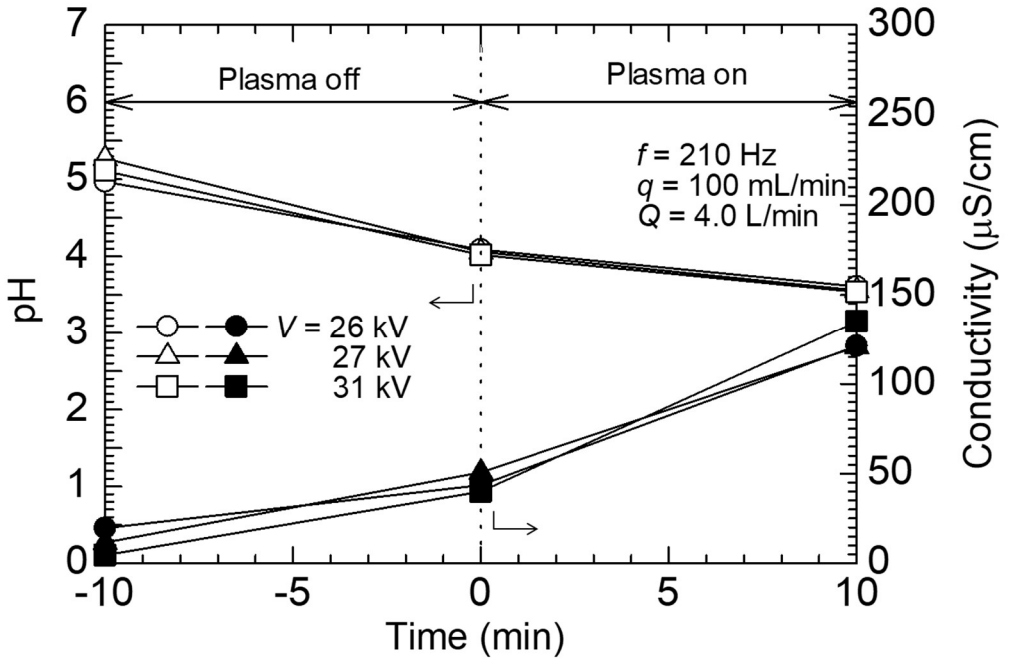
Plasma off
Plasma on
f = 210 Hz
q = 100 mL/min
Q = 4.0 L/min
V = 26 kV
27 kV
31 kV
pH
Conductivity (μS/cm)
Time (min)

(b)

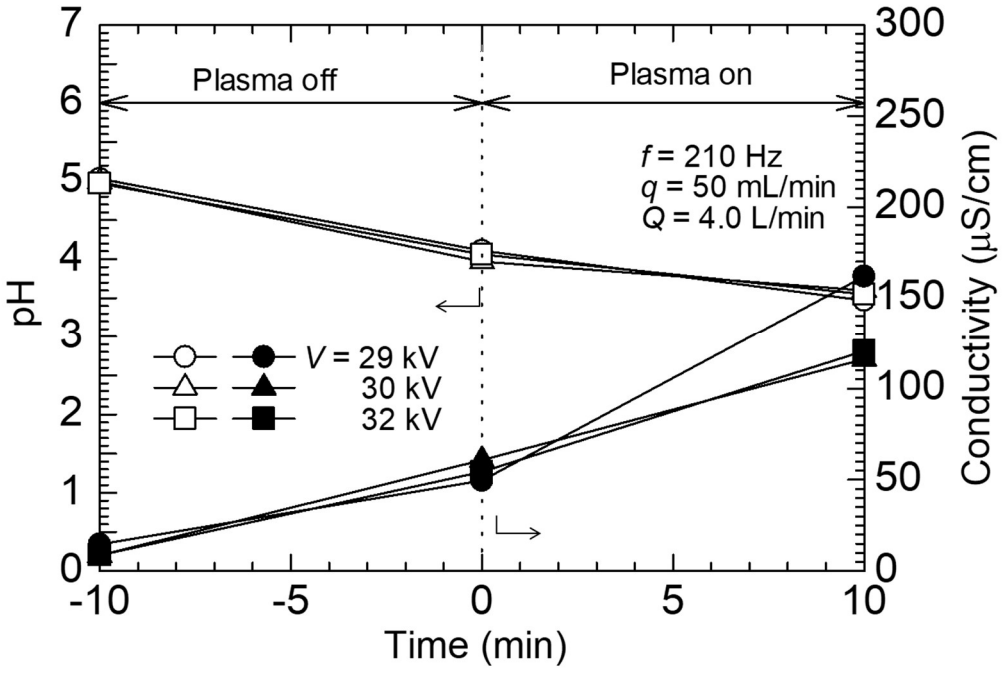
Plasma off
Plasma on
f = 210 Hz
q = 50 mL/min
Q = 4.0 L/min
V = 29 kV
30 kV
32 kV
pH
Conductivity (μS/cm)
Time (min)
0
1
2
3
4
5
6
7
0
50
100
150
200
250
300
-10
-5
0
5
10

(c)

Fig. 12

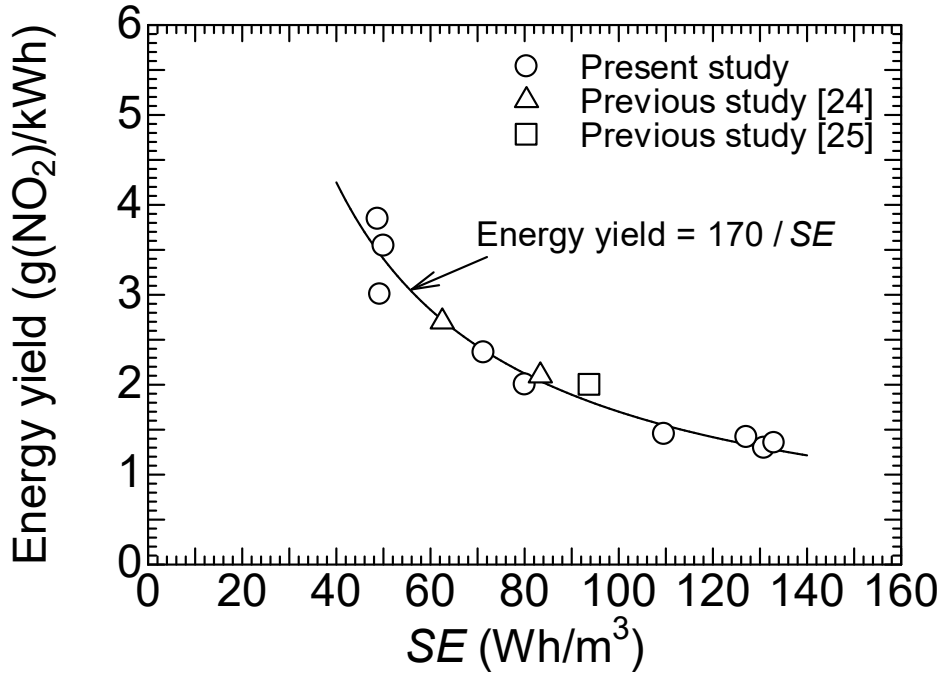
Energy yield (g(NO2)/kWh)
SE (Wh/m3)
Present study
Previous study [24]
Previous study [25]
Energy yield = 170 / SE
0
1
2
3
4
5
6
0
20
40
60
80
100
120
140
160

Fig. 13